Applied Physics A (2022) 128:1065
https://doi.org/10.1007/s00339-022-06228-y

Applied Physics A
Materials Science & Processing

Synthesis, characterization and photocatalytic properties of $In_{2.77}S_4$/Ti_3C_2 composites

Jin-Peng Liu[1] · Yun-Xuan Fu[1,2] · Ze-Hong Wang[1] · Xiao-Ye Ma[1] · Xiang-Feng Wu[1] · Hong-Yang Li[1] · Ye-Wei Kang[1] · Hui Wang[1] · Li-Jie Ci[3]

Received: 2 September 2022 / Accepted: 7 November 2022 / Published online: 14 November 2022

Abstract

Recently, the problem of water pollution, caused by antibiotics, is becoming more and more serious. Photocatalysis is one of the promising technologies for removing antibiotics from water. Herein, the $In_{2.77}S_4/Ti_3C_2$ composites were prepared by an in-situ hydrothermal growth method for photocatalytic degradation of tetracycline (TC). The as-developed composites were characterized by various methods. The UV–Vis DRS spectra reveals that the introduction of Ti_3C_2 makes the bandgap of the as-prepared composites smaller and the visible light absorption ability improved. The photocatalytic degradation efficiency of the as-prepared composite is enhanced under visible light illumination. It is shown as first increasing and then decreasing with increasing the content of Ti_3C_2 in the composite and reaches to the maximum of 89.3% in 90 min, which is higher than 75.1% of $In_{2.77}S_4$ and 6.7% of Ti_3C_2. The reason of improvement is the interface between $In_{2.77}S_4$ and Ti_3C_2 is tightly combined to form a heterojunction. Moreover, the photocurrent intensity of the as-obtained composite is improved, while its Nyquist arc radius is decreased. In addition, holes are the main active species and ·OH and $\cdot O_2^-$ play an auxiliary role during the degradation of TC.

Keywords $In_{2.77}S_4$ · Ti_3C_2 · Heterojunction · Tetracycline · Photocatalysis

1 Introduction

In recent years, the market demand for antibiotics such as tetracycline (TC) has sharply increased as the increasing ability of people to pay for medical care and the pandemics such as COVID-19 spread [1, 2]. The discharge of antibiotics can result in water pollution and further threat to human health because of their relatively stable structure [3]. To solve this problem many methods such as physical adsorption, biological treatment and semiconductor photocatalysis have been developed [4]. Among above mentioned methods semiconductor photocatalysis is regarded as one of the promising and sustainable strategies. In this way, the light reaction is accelerated by the action of the photocatalyst, that is, the photocatalyst reacts with the substrate in its ground or excited state to produce light-induced products [5]. Generally speaking, the photocatalyst basically remains unchanged during the whole reaction process. This method can be used to degrade antibiotics into H_2O and CO_2 under visible light illumination [6–8]. However, the bandgap of many traditional semiconductor photocatalysts is generally greater than 3.2 eV, and their response ability to visible especially infrared light is almost negligible. As a metal sulfide with sulfur defects, $In_{2.77}S_4$ has a narrow bandgap between 1.75 eV and 2.17 eV and high photocatalytic activity for various organics, such as methylene blue (MB), methyl orange (MO) and rhodamine B (RhB) [9–18]. It still has

Jin-Peng Liu, Yun-Xuan Fu and Ze-Hong Wang have contributed equally to this work and share the first authorship.

✉ Xiang-Feng Wu
wuxiangfeng@stdu.edu.cn

✉ Hui Wang
hui-wang@stdu.edu.cn

[1] School of Materials Science and Engineering, Hebei Key Laboratory of Advanced Materials for Transportation Engineering and Environment, Shijiazhuang Tiedao University, Shijiazhuang 050043, China

[2] Tianjin Key Laboratory of Building Green Functional Materials, Tianjin Chengjian University, Tianjin 300384, China

[3] College of Chemical Engineering, Shijiazhuang University, Shijiazhuang 050035, China

some shortcomings, such as poor cycle stability and fast photogenerated electron–hole pairs recombination. To improve its disadvantages our research group has previously synthesized the composite photocatalysts by hybridizing it with other suitable semiconductors such as $SrCO_3$ [14], $In(OH)_3$ [15] and WS_2 [16] and doping it with some metallic elements such as Zn^{2+} [17] and Sn^{4+} [18].

Ti_3C_2 contains a large number of functional groups such as –OH and –O on its surface and has many advantages of good stability, high specific surface area and carriers mobility. Moreover, it has the metal conductivity of transition metal carbide, which helps it to bond closely with other semiconductors. This can accelerate the capture and transfer of photogenerated electrons and then improve their transport efficiency [19]. Many researchers have used Ti_3C_2 as a cocatalyst to prepare visible-light-driven composite photocatalysts. For example, Tan et al. have successfully prepared $Bi_2O_2CO_3/Ti_3C_2$ heterojunction composite by a hydrothermal method, and the photocatalytic degradation efficiency of the as-prepared composite for TC reached 80% [20]. Yang et al. have improved the problems of poor conductivity, easy aggregation and high photogenerated carriers recombination rate of Fe–Ni layered double hydroxides (FeNi-LDH) by hybridizing it with Ti_3C_2, and benefited from these advantages the TC removal rate of the as-prepared sample was 94.7% [21]. Han et al. have fabricated 2D/3D heterojunction photocatalyst by decorating 2D Ti_3C_2 on 3D flower-like Bi_2WO_6 nanosheets, and the as-prepared composites showed the photocatalytic degradation efficiency of 79.8% for TC hydrochloride (TC-HCl) [22].

To further improve the photocatalytic performance and cycling stability of $In_{2.77}S_4$, in this work, few-layer Ti_3C_2 nanosheets with shorter electron migration distance and more surface active sites was chosen to hybridize it by an in-situ hydrothermal growth method. Many characterization methods such as X-ray diffraction (XRD), (high-resolution) transmission electron microscopy ((HR)TEM), UV–Vis diffuse reflectance spectroscopy (UV–Vis DRS), photoluminescence (PL) and X-ray photoelectron spectroscopy (XPS) and electrochemical impedance spectroscopy (EIS) were used to investigate the relationship between micro structure and macro performance of the as-prepared samples. TC dilute solution was used to assess the photocatalytic activity of the as-prepared $In_{2.77}S_4/Ti_3C_2$ composites. Experimental results show that the photocatalytic degradation efficiency of the as-prepared composite is improved in comparison with pure samples due to the formation of heterojunction at the interface of $In_{2.77}S_4$ and Ti_3C_2. The photocatalytic degradation mechanism of the as-prepared composite for TC was also analyzed. This work can provide a guidance for the treatment of antibiotic contamination in water under sunlight.

2 Experimental section

2.1 Materials

The $In_{2.77}S_4$ nanosheets were fabricated according to our previous work [10]. *tert*-Butyl alcohol (*t*-BuOH), *p*-benzoquinone (BQ), ethylenediamine tetraacetatic acid (EDTA), 4-hydroxy-2,2,6,6-tetramethylpiperidin-1-oxyl (TEMPOL), indium nitrate hydrate ($In(NO_3)_3{\cdot}xH_2O$) and thioacetamide (TAA) were purchased from Sinopharm Chemical Reagent Co., Ltd., China. TC was purchased from Shanghai Mclean Chemical Reagent Co., Ltd., China. All chemicals were analytical reagent without any further treatment.

2.2 Preparation of few-layer Ti_3C_2 nanosheets

In a typical preparation process, 2.98 g NH_4F was mixed with 20 mL HCl for 5 min. 0.5 g Ti_3AlC_2 was added into the above mixture and the reaction temperature was kept at 40 °C. 24 h later the few-layer Ti_3C_2 nanosheets were collected using a polyethersulfone membrane, fully washed with deionized water and placed in a vacuum drying oven at 60 °C overnight.

2.3 Preparation of $In_{2.77}S_4/Ti_3C_2$ composite photocatalyst

Scheme 1 illustrates the preparation procedure of $In_{2.77}S_4/Ti_3C_2$ composites and a typical preparation process was presented as follows. 6.25 mg of the as-fabricated Ti_3C_2 powder and 0.764 g $In(NO_3)_3{\cdot}xH_2O$ were fully mixed with 40 mL of deionized water, labeled as solution 1. 0.601 g TAA was dissolved in 40 mL of deionized water, labeled as solution 2. The solution 1 was mixed with solution 2, and the as-prepared mixture were placed into a lining polytetrafluoroethylene (PTFE) hydrothermal reactor and heated in a blast drying oven at 180 °C. 12 h later the reactor was taken out and naturally cooled down to room temperature, and the sample was filtered using a polyethersulfone membrane, washed with deionized water and dried in a vacuum drying oven at 60 °C overnight. The as-prepared composite photocatalyst was named as $In_{2.77}S_4/Ti_3C_2(0.5)$. Other samples were prepared via the same process by only changing the usage of Ti_3C_2 of 1.56 mg, 3.13 mg, 9.38 mg, and they were named as $In_{2.77}S_4/Ti_3C_2$ (0.125), $In_{2.77}S_4/Ti_3C_2$ (0.25) and $In_{2.77}S_4/Ti_3C_2$ (0.75), respectively.

2.4 Characterization

The crystal structure of the as-synthesized samples was characterized using XRD (Bruker D8 ADVANCE, Germany). The

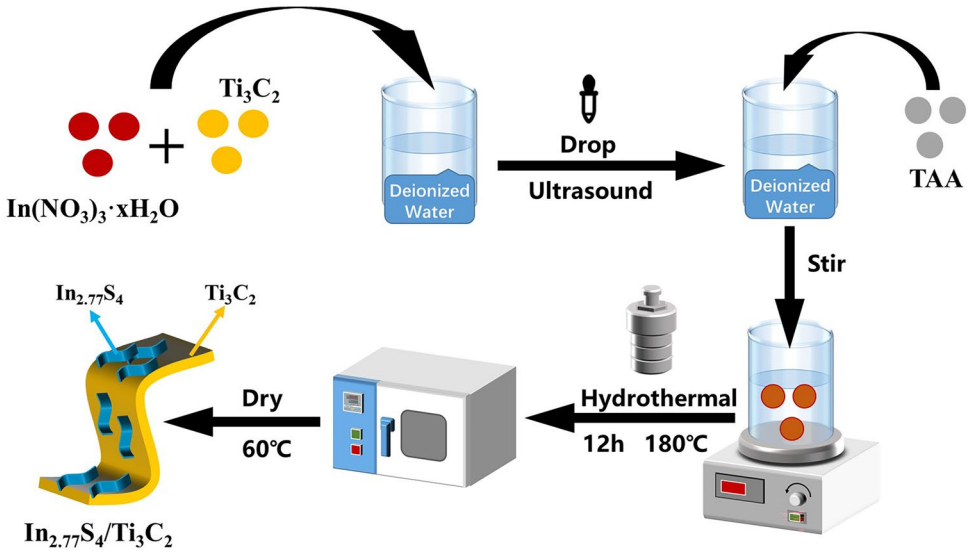

Scheme 1 Schematic illustration of preparation of $In_{2.77}S_4/Ti_3C_2$ composites

microstructure of the as-developed samples was observed by employing (HR)TEM (JEOL JEM 2100, Japan). The optical properties of as-obtained samples were analyzed by utilizing UV–Vis DRS (Hitachi U-4100, Japan). The PL spectra of the as-prepared samples were tested on a fluorescence spectrometer (Horiba FluoroMax + -4, USA). The elements valence of the as-prepared samples was detected using XPS (Thermo Scientific K-Alpha X-ray, USA). The charge transfer and separation of as-developed samples were tested using EIS (Chi760, Shanghai Chenhua Instrument Co., Ltd., China).

2.5 Photocatalytic performance tests

The photocatalytic activities of the samples were discussed by degrading TC dilute solution with the concentration of 10 mg/L under visible light illumination. Typically, 50 mg samples and 100 mL TC solution were well-mixed in a photocatalytic reactor, which was placed in dark to achieve the adsorption–desorption equilibrium. 4 mL of mixture was taken out every 20 min, placed in a centrifugal tube and irradiated under a Xe light equipped with a 420 nm ultraviolet filter (CEL-HXF300, Beijing Zhongjiao Jinyuan Technology Co., Ltd., China). The reaction solution was then transferred into a tube and centrifuged to remove the sediment (H1850, Xiangyi Centrifuge Co., Ltd., China). The supernate was collected and used to measure the absorbancy of the samples on an ultraviolet–visible spectrophotometer (722 N, Shanghai Precision Instrument Co., Ltd., China) at the wavelength of 357 nm. The degradation efficiency of photocatalyst was obtained by formula (1) [14, 15]:

$$\text{Efficiency} = C_t/C_0 \quad (1)$$

In this equation, C_0 is the initial concentration of TC and C_t is the concentration at the test time.

3 Results and discussion

3.1 XRD analysis

The XRD patterns of the samples are exhibited in Fig. 1. It can be seen that the characteristic diffraction peaks of pure $In_{2.77}S_4$ show at 23.4°, 27.5°, 28.8°, 33.3°,43.8°, 47.9°, 54.0°, 56.1°, 59.6° and 70.1°, which are consistent with (220), (311), (222), (400), (511), (440), (620), (533), (444) and (800) lattice planes of β-$In_{2.77}S_4$ according to JCPDS 88–2495, respectively [15]. Moreover, the characteristic diffraction peaks of Ti_3C_2 in the as-developed $In_{2.77}S_4/Ti_3C_2$ composites are not obvious. This may be due to the high

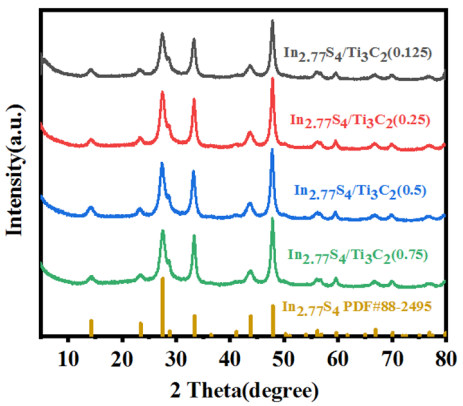

Fig. 1 XRD patterns of $In_{2.77}S_4/Ti_3C_2$ composites with different content of Ti_3C_2

dispersion and relatively low content of Ti_3C_2 in the composites [21]. In addition, no other impurity diffraction peaks appear in the samples. This means the samples are pure.

3.2 Photocatalytic performances analysis

It can be seen from the dark adsorption curves in Fig. 2a that all sample reach the adsorption–desorption equilibrium in 60 min. When the samples are exposed to visible light, as shown in Fig. 2b, the photocatalytic degradation efficiencies of $In_{2.77}S_4$ and Ti_3C_2 are 75.1% and 6.7%, respectively. It is found that the introduction of Ti_3C_2 improves the degradation efficiency of $In_{2.77}S_4$ under the visible light irradiation. Moreover, with increasing the content of Ti_3C_2 in the as-prepared composite samples, the degradation efficiency of the $In_{2.77}S_4/Ti_3C_2$ composite photocatalyst shows a trend of increasing initially and then decreasing. When the content of Ti_3C_2 is 6.25 mg, the $In_{2.77}S_4/Ti_3C_2$ composite photocatalyst has the best degradation efficiency of 89.3% in 90 min. This is higher than 75.1% of $In_{2.77}S_4$ and 6.7% of Ti_3C_2, respectively. Moreover, the reaction rate of each sample, shown in Fig. 2c, has a good linear relation, which is consistent with the results of first-order kinetic fitting curves. Furthermore, the curve slope of the $In_{2.77}S_4/Ti_3C_2(0.5)$ composite is the largest. This result indicates that the as-developed $In_{2.77}S_4/Ti_3C_2(0.5)$ composite has the best photocatalytic degradation efficiency. In addition, in Fig. 2d, it can be seen that with the increase of reaction time, the peak intensity of the characteristic peak of TC at 357 nm gradually decreases during the photocatalytic reaction process. This experimental result is consistent with Fig. 2a, b.

3.3 TEM analysis

The TEM image in Fig. 3a shows that the as-prepared $In_{2.77}S_4$ particles are irregular nanosheets with the diameter of 30–50 nm. In Fig. 3b, it shows Ti_3C_2 are few-layer nanosheets with the diameter of 50–200 nm. Meanwhile, it can be observed in Fig. 3c that the as-developed composites are small nanosheets of $In_{2.77}S_4$ evenly loading on the larger Ti_3C_2 nanosheets. In Fig. 3d, it can be observed that there are two widths of lattice fringes of 0.309 nm and 0.99 nm,

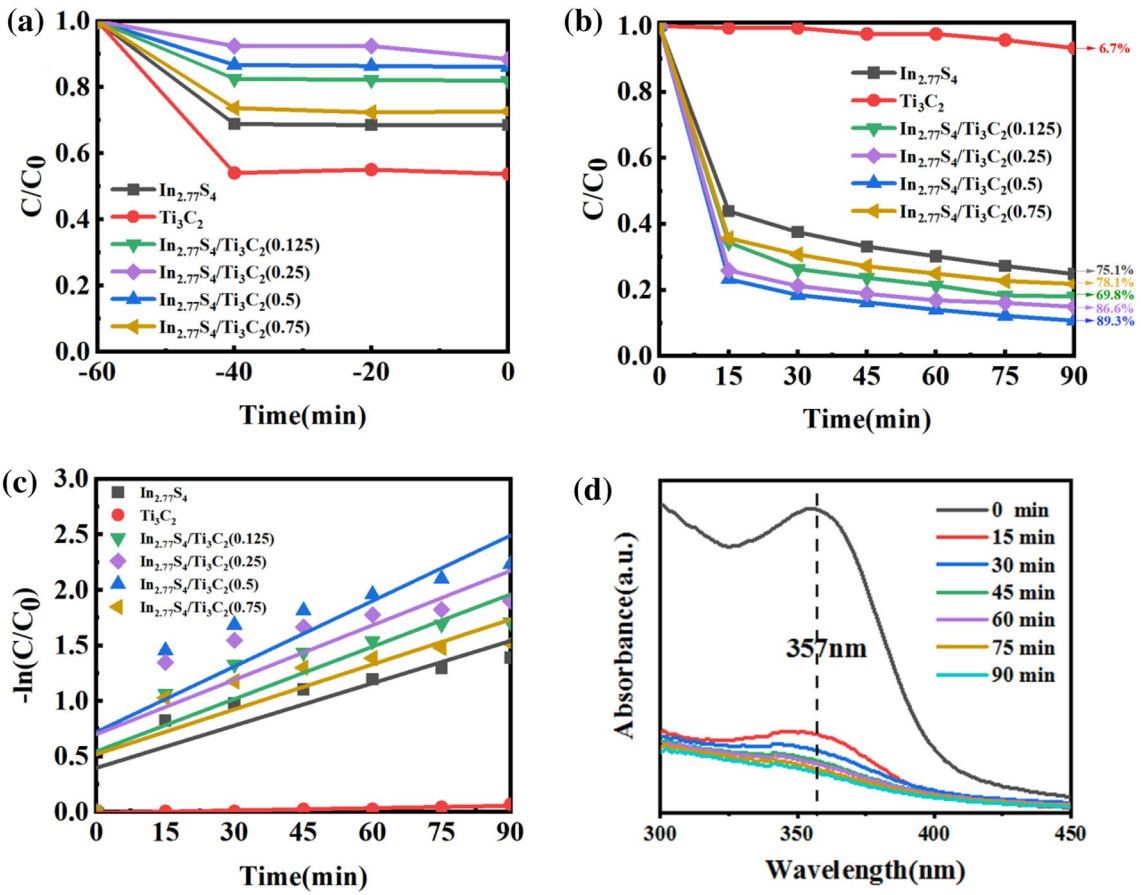

Fig. 2 **a** Dark adsorption efficiency of the samples for TC degradation. **b** Photocatalytic degradation efficiency of the samples for TC degradation. **c** First-order kinetic fitting curves of the samples. **d** UV–Vis absorption spectra of $In_{2.77}S_4/Ti_3C_2(0.5)$ composite for photocatalytic degradation of TC in different time

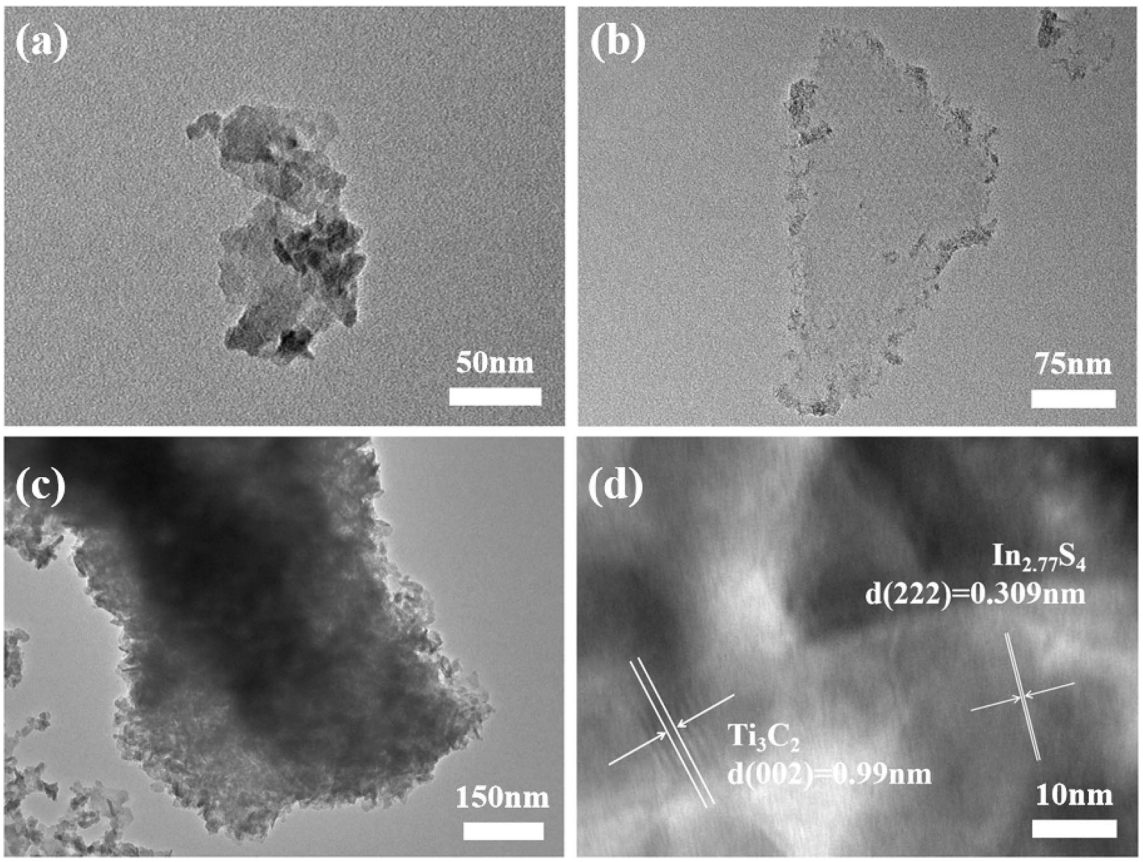

Fig. 3 TEM images of **a** $In_{2.77}S_4$, **b** Ti_3C_2 and **c** $In_{2.77}S_4/Ti_3C_2(0.5)$ composite. HRTEM image of **d** $In_{2.77}S_4/Ti_3C_2(0.5)$ composite

which are corresponding to the (222) plane of $In_{2.77}S_4$ and the (002) plane of Ti_3C_2, respectively. These results demonstrate that the heterojunction exists in the interface of the $In_{2.77}S_4/Ti_3C_2(0.5)$ composite. This structure is beneficial for improving the separation of photo-generated electron–hole pairs of the composites.

3.4 UV–Vis DRS analysis

In Fig. 4a, it can be seen that the absorption peak of the as-prepared composite shows a slight red shift in comparison with pure $In_{2.77}S_4$. This result demonstrates that Ti_3C_2 contributes to the increase of the photoresponse range of

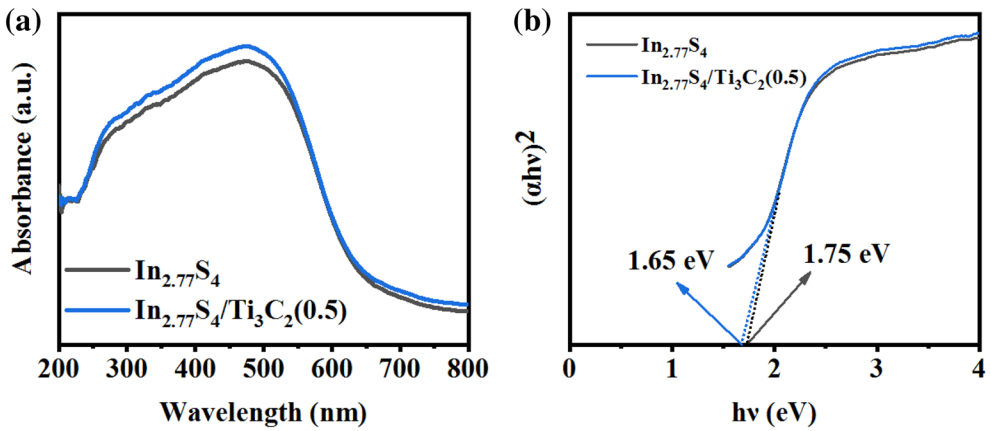

Fig. 4 **a** UV–Vis DRS spectra and **b** plots of $(\alpha hv)^2$ versus hv of $In_{2.77}S_4$ and $In_{2.77}S_4/Ti_3C_2(0.5)$ composite

$In_{2.77}S_4$, and its light absorption intensity is enhanced. The bandgap diagram of the sample is shown in Fig. 4b, and the bandgap value can be calculated by formula (2) [22–24]:

$$\alpha h\nu = A(h\nu - E_g)^{n/2} \quad (2)$$

In this formula, α, ν, A and E_g represent absorption coefficient, frequency, constant and forbidden band width, respectively. In general, the value of n is related to the conversion type of the semiconductor. In this work, $In_{2.77}S_4$ is a direct transition semiconductor and n is equal to 1 [24–26]. In Fig. 4b, it can be found that the forbidden band width of $In_{2.77}S_4$ is 1.75 eV and that of the as-prepared $In_{2.77}S_4/Ti_3C_2(0.5)$ composite is 1.65 eV. This result means that the introduction of Ti_3C_2 makes the bandgap of the as-prepared composite smaller and has strengthened the visible light absorption ability of $In_{2.77}S_4$.

3.5 XPS analysis

Figure 5 shows XPS survey spectra of the samples and Table 1 shows the chemical bonds or orbitals corresponding to specific binding energies of the samples. It can be seen in Fig. 5a that in the as-prepared $In_{2.77}S_4/Ti_3C_2(0.5)$ composite, except for the O element from the surface contamination of the sample, it contains four elements of S, In, Ti, and C, and no other impurity elements are detected. This indicates that the $In_{2.77}S_4/Ti_3C_2(0.5)$ composite is purity. Figure 5b and Table 1 illustrate that the binding energies of Ti_3C_2 at

Table 1 Chemical bonds or orbitals corresponding to specific binding energies of the samples [14–18, 27, 28]

Chemical bonds or orbitals	Pure samples	$In_{2.77}S_4/Ti_3C_2(0.5)$ composite
	Binding energy (eV)	
S $2p_{3/2}$	161.7	161.6
S $2p_{1/2}$	162.9	162.9
O–C=O	164.4	289.1
C–Ti	281.6	282.3
C–C	284.8	284.8
C–O	286.5	286.5
In $3d_{5/2}$	445.1	445.0
In $3d_{3/2}$	452.6	452.5

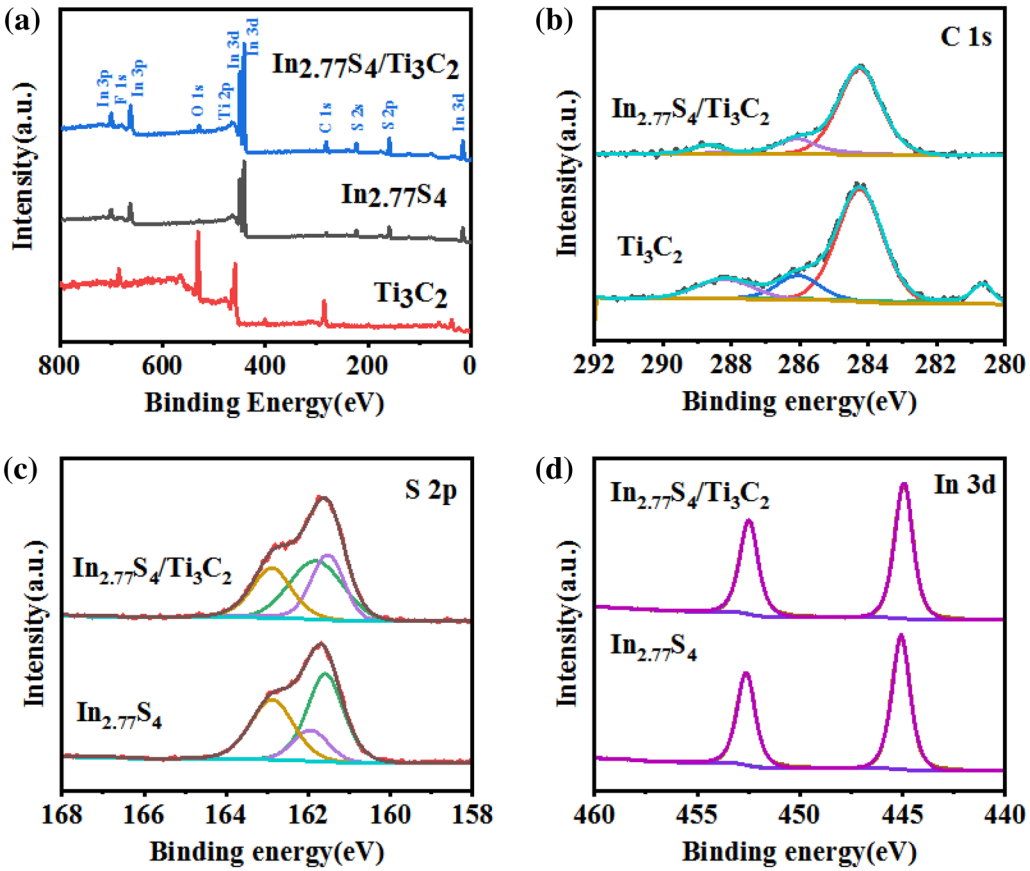

Fig. 5 **a** XPS survey spectra of the samples. High-resolution XPS spectra of the samples: **b** C 1s, **c** S 2p and **d** In 3d

281.6 eV, 284.8 eV, 286.5 eV and 164.4 eV, which are correspond to the C–Ti, C–C, C–O and O–C=O bonds of C 1 s, respectively. The corresponding binding energies of the bonds in the $In_{2.77}S_4/Ti_3C_2$(0.5) composite are 282.3 eV, 284.8 eV, 286.5 eV and 289.1 eV. The presence of the C–Ti bond is located at 282.3 eV. Although the peak intensity is weak it indicates the presence of Ti_3C_2 in the as-prepared composite [27, 28]. As shown in Fig. 5c, d and Table 1, the binding energies of $In_{2.77}S_4/Ti_3C_2$(0.5) at 161.6 eV and 162.9 eV in S 2p map belongs to S $2p_{3/2}$ and S $2p_{1/2}$ orbitals. The binding energies at 445.0 eV and 452.5 eV in the In 3d map belong to the In $3d_{5/2}$ and In $3d_{3/2}$ spin orbits. The four binding energies corresponding to pure $In_{2.77}S_4$ are 445.1 eV and 452.6 eV, 161.7 eV and 162.9 eV, respectively [14–18]. Compared with the pure samples, all of three peaks of $In_{2.77}S_4/Ti_3C_2$(0.5) are slightly moved. The above results prove that the interaction between the two pure samples in the composites is not a simple physical contact, but a chemical bond contact [29, 30]. This structure is beneficial of the rapid migration of electrons and reducing the surface energy of the as-developed composite photocatalyst.

The XPS valence band (VB) and the schematic illustration of the bandgap energy diagram of $In_{2.77}S_4$ and $In_{2.77}S_4/Ti_3C_2$(0.5) composite are shown in Fig. 6. It can be seen that the VB positions of $In_{2.77}S_4$ and $In_{2.77}S_4/Ti_3C_2$(0.5) are 1.62 eV and 1.58 eV, respectively. Combining the VB value and the forbidden band width of the sample can calculate the conduction band (CB) positions of the samples by formulas (3) and (4) [31, 32]:

$$E_{CB} = \chi - E_e - 0.5E_g \tag{3}$$

$$E_{VB} = E_g + E_{CB} \tag{4}$$

where E_{VB}, E_{CB}, χ, and E_e are VB energy (E_{VB}), CB energy (E_{CB}), absolute electronegativity and energy of free electrons, respectively. According to above formulas, the CB positions of $In_{2.77}S_4$ and $In_{2.77}S_4/Ti_3C_2$(0.5) are -0.13 eV and 0.07 eV, respectively.

3.6 Photoelectrochemical analysis

In Fig. 7a, it can be seen that the transient photocurrent intensity of the $In_{2.77}S_4/Ti_3C_2$(0.5) composite is higher than that of two pure samples. Specifically, the as-prepared composite sample is about 3 times of $In_{2.77}S_4$ and 50 times

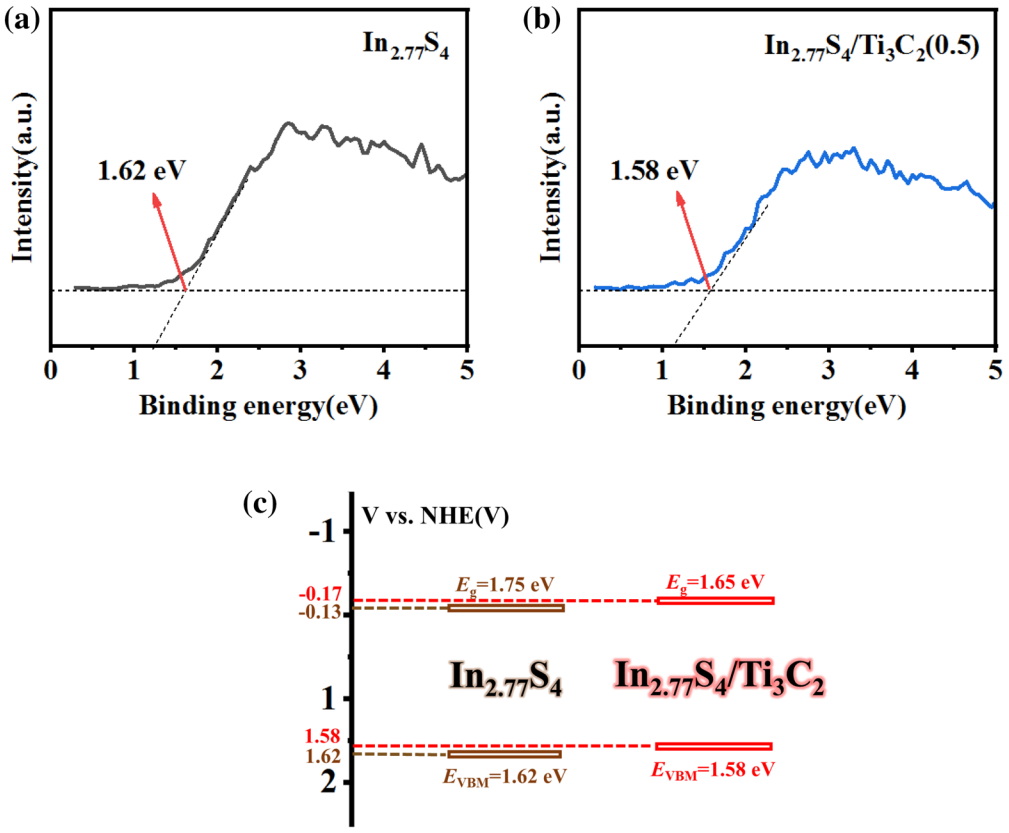

Fig. 6 XPS valence band diagram of **a** $In_{2.77}S_4$, **b** $In_{2.77}S_4/Ti_3C_2$(0.5) composite and **c** schematic illustration of the bandgap energy diagram of $In_{2.77}S_4$ and $In_{2.77}S_4/Ti_3C_2$(0.5) composite

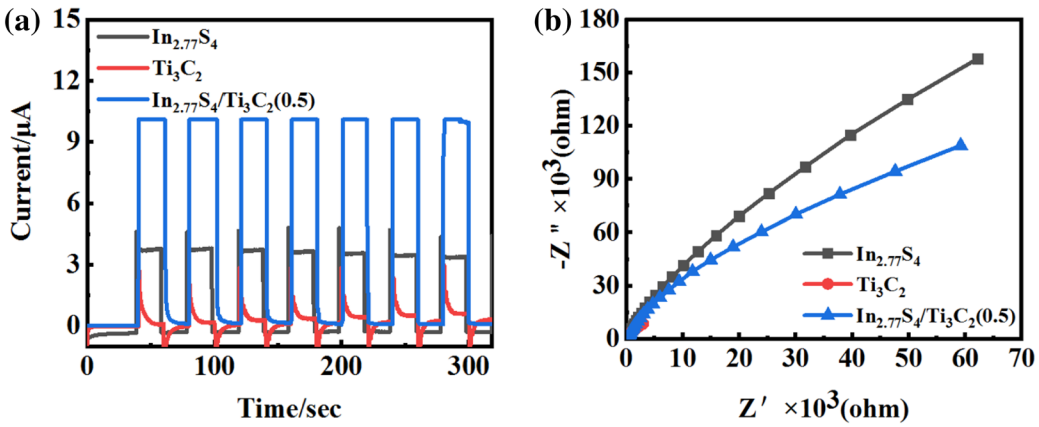

Fig. 7 **a** Transient photocurrent density response and **b** EIS spectra of the samples

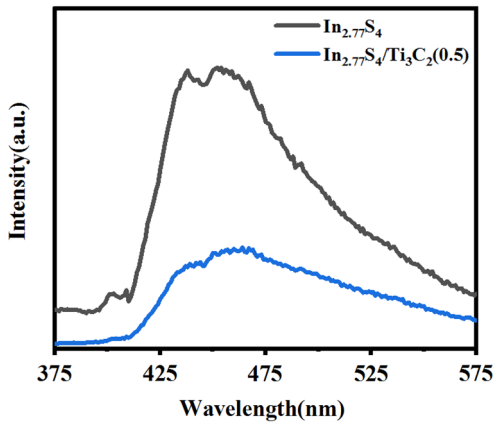

Fig. 8 PL spectra of $In_{2.77}S_4$ and $In_{2.77}S_4/Ti_3C_2(0.5)$ composite

of Ti_3C_2. Moreover, in Fig. 7b, its internal resistance is almost zero due to the high conductivity of Ti_3C_2. After it is hybridized with $In_{2.77}S_4$, the Nyquist arc radius of the $In_{2.77}S_4/Ti_3C_2(0.5)$ composite is smaller than that of pure $In_{2.77}S_4$. This shows that the charge transport resistance of the as-developed composite is reduced, and the separation rate of photogenerated electron–hole pairs is improved. This result reveals that the recombination of $In_{2.77}S_4$ and Ti_3C_2 can improve the lifetime of the photogenerated electron–hole pairs in comparison of $In_{2.77}S_4$.

3.7 PL analysis

It can be found in Fig. 8 that the peak of the $In_{2.77}S_4/Ti_3C_2(0.5)$ composite is reduced in comparison with that of $In_{2.77}S_4$ when the excitation wavelength is 325 nm. This means that the recombination rate of photogenerated electron–hole pairs of the as-prepared composite is reduced. It also indicates that the charge separation efficiency of $In_{2.77}S_4/Ti_3C_2(0.5)$ composite is better than that of $In_{2.77}S_4$.

3.8 Cyclic stability analysis

Cyclic stability is usually regarded as an important parameter for whether photocatalysts can be popularized in practice [33–35]. As shown in Fig. 9a, after 3 cycles, the degradation efficiency of pure $In_{2.77}S_4$ to TC solution is 42.3%, which is lower than 65.1% of the first cycle. Meanwhile, that of $In_{2.77}S_4/Ti_3C_2(0.5)$ composite sample reaches to 63.5%, which is lower than 89.3% of the first cycle. However, it is higher by 21.2% than pure $In_{2.77}S_4$. In Fig. 9b, it can be seen that the structure is no obvious change for samples before and after 3 cycles. This phenomenon shows that the composition and crystal structure of the $In_{2.77}S_4/Ti_3C_2(0.5)$ composite photocatalyst have not been obviously changed before and after 3 cycles. Moreover, it also means the introduction of Ti_3C_2 is beneficial to improving the cycle stability of $In_{2.77}S_4$.

3.9 Photocatalytic degradation mechanism analysis

To provide the photocatalytic degradation mechanism of the as-developed $In_{2.77}S_4/Ti_3C_2(0.5)$ hybrid, 0.5 mmol *t*-BuOH, EDTA·2Na, TEMPOL are respectively used to trap hydroxyl radicals (·OH), holes and superoxide radicals ($\cdot O_2^-$), respectively [36, 37]. As exhibited in Fig. 10, after using EDTA·2Na and *t*-BuOH, the photocatalytic degradation efficiency is significantly inhibited, and the degradation efficiency of TC solution decreases to 0% and 68.8%, respectively. However, when TEMPOL is added, the photocatalytic degradation efficiency is the highest of 89.3%. Therefore, the holes are the main active free radicals in the degradation of TC solution, while ·OH and $\cdot O_2^-$ are secondary and tertiary active substances, respectively.

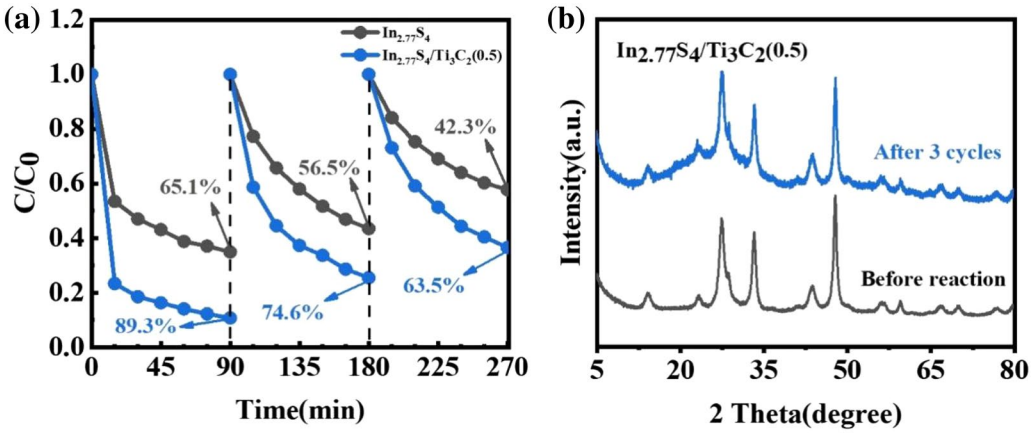

Fig. 9 **a** Cycling stability of $In_{2.77}S_4$ and $In_{2.77}S_4/Ti_3C_2(0.5)$ composite for TC degradation and **b** XRD patterns of $In_{2.77}S_4/Ti_3C_2(0.5)$ composite for TC degradation before reaction and after 3 cycles

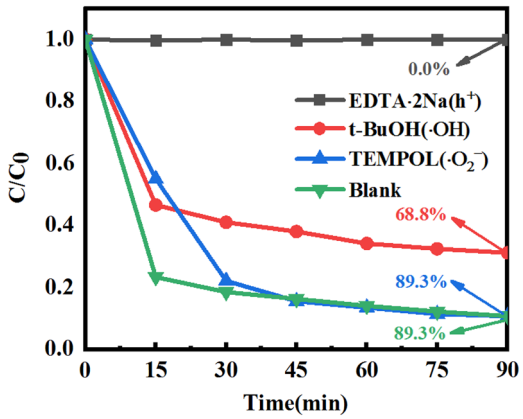

Fig. 10 Photocatalytic degradation curves of $In_{2.77}S_4/Ti_3C_2(0.5)$ composite with using different scavengers

Combined with above analysis results the possible photodegradation mechanism of $In_{2.77}S_4$ and the as-prepared $In_{2.77}S_4/Ti_3C_2$ for TC can be provided, as shown in Fig. 11. Under visible light irradiation, the (111), (220), (311), (222), (400), (511), (440), (533), (444) and (800) crystal faces expose to $In_{2.77}S_4$ excite and generate electrons at VB and holes at CB. The holes accumulated at the VB of $In_{2.77}S_4$ can directly oxidize TC molecules into small molecular products such as H_2O and CO_2 or react with H_2O to form ·OH, which can further participate in catalytic degradation process under visible light illumination. For the $In_{2.77}S_4/Ti_3C_2(0.5)$ composite, on the one hand, the photogenerated electrons can react with O_2, on the surfaces of the samples, to generate $\cdot O_2^-$ and then oxidize TC. On the other hand, its degradation mechanism in VB is similar to that of pure $In_{2.77}S_4$. The aim of this work is to adjust the band edge position and bandgap by constructing $In_{2.77}S_4/Ti_3C_2$ heterojunction (the VB and CB of $In_{2.77}S_4$ is 1.62 eV and -0.13 eV, respectively; the VB and CB of

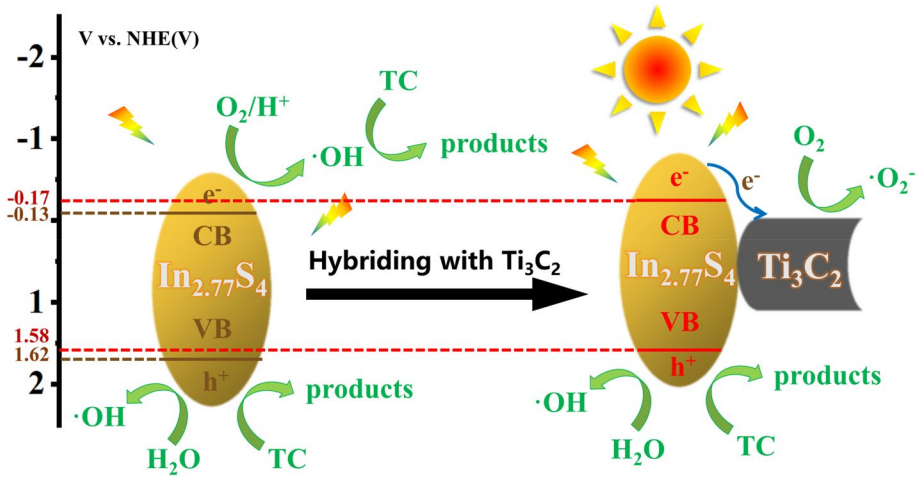

Fig. 11 Photocatalytic degradation mechanism of $In_{2.77}S_4$ and $In_{2.77}S_4/Ti_3C_2(0.5)$ composite for TC

$In_{2.77}S_4/Ti_3C_2$ VB is 1.58 eV and -0.17 eV, respectively). This helps to enhance photocatalytic activity and increase oxidation capacity of pure $In_{2.77}S_4$. It is also worth emphasizing that such interfacial connections will theoretically construct charge-transfer channels, facilitate electron–hole pairs separation and then improve the efficiency of photocatalytic degradation of the as-developed $In_{2.77}S_4/Ti_3C_2$ composite.

4 Conclusions

In summary, $In_{2.77}S_4/Ti_3C_2$ composites, as a visible-light-driven photocatalyst, were prepared by an in-situ growth hydrothermal method and TC was used to evaluate the photocatalytic activity of the as-prepared samples. Experimental results show that the photocatalytic activity of $In_{2.77}S_4$ can be enhanced by loading few-layer Ti_3C_2 nanosheets. This improvement is because the interface between $In_{2.77}S_4$ and Ti_3C_2 is tightly combined to form a heterojunction and then improve the charge separation efficiency of the as-developed composite. Moreover, the photocurrent intensity of the as-prepared composite photocatalyst is increased about three times, while the electrochemical impedance is decreased. In addition, the holes are the main active substance in the degradation of TC solution, while ·OH and $\cdot O_2^-$ are secondary and tertiary ones, respectively. This work will not only provide a different insight for improving the disadvantages of $In_{2.77}S_4$, but also supply a reference for treating wastewater under sunlight.

Author contributions All authors contributed to the study conception and design. The manuscript was written by J-PL. Material preparation, data collection and analysis were performed by Y-XF, Z-HW, X-YM, X-FW, H-YL, Y-WK and L-JC. The review and supervision were performed by X-FW and HW. All authors read and approved the final manuscript.

Funding This work was financially supported by the Natural Science Foundation of Hebei Province, China (Nos. E2019210251 and B2019210331), the Innovation Ability Improvement Project of Hebei Province, China (No. 20543601D) and the Ministry of Education 'Chun Hui Plan' Cooperative Research Project, China.

Data availability The authors declare that the data supporting the findings of this study are available within the article.

Declarations

Conflict of interest The authors declare that there are no conflicts of interest.

Research involving human and/or animal participants This article does not contain any studies with human participants or animals performed by any of the authors.

References

1. Y.Y. He, D.B. Wang, X.P. Li, Q.Z. Fu, L. Yin, Q. Yang, H. Chen, Chemosphere **284**, 131386 (2021)
2. H. Zhang, L. Zhou, J. Li, S.J. Rong, S.Q. Liu, Front. Chem. **8**, 593730 (2021)
3. Z.W. Ye, S. Feng, W. Wu, Y. Zhou, Y. Wang, X.J. Dai, X. Cao, Solid State Sci. **127**, 106842 (2022)
4. X. Meng, L. Yan, M. Wei, T. Wang, T. Xu, Y. Yan, S. Cheng, N. J. Chem. **45**, 16355 (2021)
5. R. Abazari, S. Sanati, A. Morsali, A.M. Kirillov, Inorg. Chem. **13**, 9660 (2021)
6. Y.F. Wang, Z. Li, M. Jiang, X. Yu, L. Xu, Sci. Total Environ. **846**, 157470 (2022)
7. L. Wang, X.L. Ma, G.F. Huang, R. Lian, J.W. Huang, H.D. She, Q.Z. Wang, J. Environ. Sci. **112**, 59 (2022)
8. X.Q. Shi, L.N. Wang, A.A. Zuh, Y.F. Jia, F. Ding, H.F. Cheng, Q.Z. Wang, J. Alloys Compd. **903**, 163889 (2022)
9. L.Q. Shao, J. Li, X.M. Liang, T. Xie, S.C. Meng, D.L. Jiang, M. Chen, RSC. **6**, 18227 (2016)
10. X.F. Wu, H. Li, Y. Sun, Y.J. Wang, C.X. Zhang, X.D. Gong, Y.D. Wang, Y. Liu, X.Y. Yang, Appl. Phys. A. **123**, 426 (2017)
11. X.F. Wu, Y. Sun, H. Li, Y.J. Wang, C.X. Zhang, J.R. Zhang, J.Z. Su, Y.W. Wang, Y. Zhang, C. Wang, M. Zhang, J. Alloy. Compd. **740**, 1197 (2018)
12. X.F. Wu, Y.J. Wang, L.J. Song, J.Z. Su, J.R. Zhang, Y.N. Jia, J.L. Shang, X.W. Nian, C.Y. Zhang, X.G. Sun, J. Mater. Sci. Mater. El. **30**, 14987 (2019)
13. H. Li, X.F. Wu, Y. Sun, Z.H. Zhao, C.X. Zhang, F.F. Jia, H. Zhang, M.T. Yu, X.Y. Yang, JNN. **18**, 999 (2018)
14. X.F. Wu, H. Li, L.J. Song, J.Z. Su, J.R. Zhang, W.G. Zhang, M. Zhang, G.W. Sun, L. Zhan, M. Zhang, Appl. Phys. A. **124**, 584 (2018)
15. X.F. Wu, H. Li, J.Z. Su, J.R. Zhang, Y.M. Feng, J.C. Pan, Y. Zhang, L.S. Sun, W.G. Zhang, G.W. Sun, J. Nanopart. Res. **20**, 155 (2018)
16. X.F. Wu, H. Li, J.Z. Su, J.R. Zhang, Y.M. Feng, Y.N. Jia, L.S. Sun, W.G. Zhang, M. Zhang, C.Y. Zhang, Appl. Surf. Sci. **473**, 992 (2018)
17. H. Li, X.F. Wu, C.Y. Zhang, J.Z. Su, H. Wang, Z.F. Liu, Y.M. Shi, Y.Q. Zuo, Z.D. Wang, Y.X. Zhang, Appl. Phys. A. **125**, 763 (2019)
18. H. Wang, C.Y. Zhang, T.L. Chang, J.Z. Su, X.F. Wu, M.C. Song, L.L. Wang, H. Yang, L.J. Ci, J. Mater. Sci. Mater. El. **32**, 2822 (2021)
19. H.S. Huang, X. Jiang, N.J. Li, D.Y. Chen, Q.F. Xu, H. Li, J.H. He, Appl. Catal. B. **284**, 119754 (2021)
20. B.H. Tan, Y. Fang, Q.L. Chen, X.Q. Ao, Y. Cao, J. Colloid Interface Sci. **601**, 581–593 (2021)
21. L. Yang, L. Li, Z.T. Liu, C. Lai, X.F. Yang, X.X. Shi, S.Y. Liu, M.M. Zhang, Y.K. Fu, Chemosphere **294**, 133736 (2022)
22. Z.H. Han, X.X. Zhang, Y. Zuo, H.J. Dong, H.J. Ren, Sep. Purif. Technol. **299**, 121715 (2022)
23. L. Tie, S.Y. Yang, C.F. Yu, H. Chen, Y.M. Liu, S.Y. Dong, J.Y. Sun, J.H. Sun, J. Colloid Interface Sci. **545**, 63 (2019)
24. F. Chang, X.Y. Zhang, C. Yang, Appl. Surf. Sci. **527**, 11 (2020)
25. D.L. Jiang, L.L. Chen, J.J. Zhu, M. Chen, W.D. Shi, J.M. Xie, Dalton Trans. **42**, 15726 (2013)
26. Z. Qiao, T.J. Yan, W.J. Li, B.J. Huang, N. J. Chem. **41**, 3134 (2017)
27. Y. Zhao, M.D. Que, J. Chen, C.L. Yang, J. Mater. Chem. C **8**, 16258 (2020)
28. Z.P. Zeng, Y.B. Yan, J. Chen, P. Zan, Q.H. Tian, P. Chen, Adv. Funct. Mater. **29**, 1806500 (2019)

29. H. Xin, A. Lin, Y. Hu, Y.G. Li, C.Y. Hou, H.Z. Wang, Q.H. Zhang, Appl. Catal. B. **265**, 118539 (2019)
30. Z.Z. Tian, Z.L. Qi, Y.H. Yang, H.L. Yang, Q.Q. Chen, Q. Zhong, Inorg. Chem. Front. **7**, 3727 (2020)
31. N. Tian, H.W. Huang, Y.X. He, Y.X. Guo, T.R. Zhang, Y.H. Zhang, Dalton Trans. **44**, 4297 (2019)
32. Z.M. He, M.S. Siddique, H.P. Yang, Y.M. Xia, J.B. Su, B. Tang, L.N. Wang, L. Kang, Z.Y. Huang, J. Clean. Prod. **339**, 130634 (2022)
33. L. Wang, P. Wang, B.B. Huang, X.J. Ma, G. Wang, Y. Dai, X.Y. Zhang, X.Y. Qin, Appl. Surf. Sci. **391**, 557 (2017)
34. L.G. Jiang, J.Y. Chen, Y. Wang, K. Sun, F.Y. Liu, Y.Q. Lai, Mater. Lett. **224**, 109 (2018)
35. G.G. Liu, G.X. Zhao, W. Zhou, Y.Y. Liu, H. Pang, H.B. Zhang, D. Hao, X.G. Meng, P. Li, Adv. Funct. Mater. **26**, 6822 (2016)
36. H.L. Jiang, M.L. Li, J. Liu, X.Q. Li, L. Tian, P.H. Chen, Ceram. Int. **44**, 2709 (2018)
37. J.R. Ran, G.P. Gao, F.T. Li, T.Y. Ma, A.J. Du, S.Z. Qiao, Nat. Commun. **8**, 13907 (2017)